Crystallization and preliminary X-ray diffraction analysis of iron regulatory protein 1 in complex with ferritin IRE RNA

Anna I. Selezneva,[a] Giorgio Cavigiolio,[b] Elizabeth C. Theil,[b] William E. Walden[a] and Karl Volz[a]*

[a]Department of Microbiology and Immunology, University of Illinois at Chicago, Chicago, Illinois 60612-7334, USA, and [b]Children's Hospital Oakland Research Institute, Oakland, California 94609-1673, USA

Correspondence e-mail: kvolz@uic.edu

Iron regulatory protein 1 (IRP1) is a bifunctional protein with activity as an RNA-binding protein or as a cytoplasmic aconitase. Interconversion of IRP1 between these mutually exclusive states is central to cellular iron regulation and is accomplished through iron-responsive assembly and disassembly of a [4Fe–4S] cluster. When in its apo form, IRP1 binds to iron responsive elements (IREs) found in mRNAs encoding proteins of iron storage and transport and either prevents translation or degradation of the bound mRNA. Excess cellular iron stimulates the assembly of a [4Fe–4S] cluster in IRP1, inhibiting its IRE-binding ability and converting it to an aconitase. The three-dimensional structure of IRP1 in its different active forms will provide details of the interconversion process and clarify the selective recognition of mRNA, Fe–S sites and catalytic activity. To this end, the apo form of IRP1 bound to a ferritin IRE was crystallized. Crystals belong to the monoclinic space group $P2_1$, with unit-cell parameters $a = 109.6$, $b = 80.9$, $c = 142.9$ Å, $\beta = 92.0°$. Native data sets have been collected from several crystals with resolution extending to 2.8 Å and the structure has been solved by molecular replacement.

1. Introduction

The iron regulatory proteins (IRPs) are central mRNA regulators of animal cell iron metabolism (Eisenstein, 2000). IRPs bind to a family of conserved mRNA structures (Addess *et al.*, 1997; Gdaniec *et al.*, 1998), called iron responsive elements (IREs), found in a group of mRNAs that encode proteins involved in iron storage, transport and utilization. IRP/IRE binding controls either mRNA translation or mRNA degradation, depending upon the location of the IREs. Two IRPs have been identified, known as IRP1 and IRP2. The specificity of IRP–IRE interactions in each mRNA (Ke *et al.*, 1998; Gunshin *et al.*, 2000) creates a combinatorial array with graded responses to iron and oxygen signals (Theil & Eisenstein, 2000). IRP1 (MW 98.5 kDa; 889 residues) is a dual function protein: it is a regulatory RNA-binding protein with picomolar affinity while in its apo state, but assumes the function of a cytoplasmic aconitase (c-aconitase) once an iron–sulfur cluster is assembled (Kennedy *et al.*, 1992). The structure of c-aconitase has recently been solved (Dupuy *et al.*, 2006). Hence, IRP1 interconverts among three structural forms: an aconitase state, an apo form and an RNA-bound conformation.

Control of structural interconversion of IRP1 depends on iron. Low cellular levels of iron maintain IRP1 in the IRE-binding apo form of IRP1, while abundant iron favors Fe–S cluster formation and the catalytically active c-aconitase state. IRE binding by IRP1 has two metabolic consequences. Sequestration of the IRE stem-loop in mRNA prevents translation of a group of mRNAs encoding proteins that function in iron efflux, iron storage, heme biosynthesis and the tricarboxylic acid cycle and enhances iron uptake by stabilizing the transferrin receptor mRNA.

Several lines of evidence indicate that IRP1 undergoes significant structural rearrangements upon interconversion between its apo form and Fe–S cluster-containing form. Firstly, the fact that IRE binding itself is so markedly affected by the presence or absence of the Fe–S cluster while the cluster ligands are not involved in IRE binding
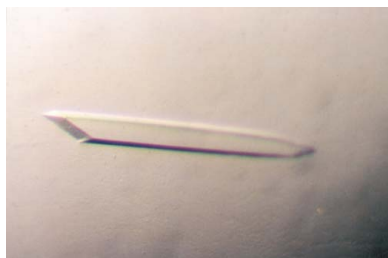
argues strongly for a conformation-driven switch (Philpott *et al.*, 1994; Hirling *et al.*, 1994). Secondly, the apo form of IRP1 is much more protease-sensitive than the holo form (Swenson & Walden, 1994; Schalinske *et al.*, 1997). Thirdly, the two forms of IRP1 have markedly different CD spectra and radii of gyration, supporting a significant difference in conformation (Brazzolotto *et al.*, 2002).

IRP1 is an important model for post-transcriptionally regulated gene-expression systems, but at present there is no X-ray structural information concerning IRP1 complexed with IRE. To investigate the conformational mechanisms underlying the different functionalities of IRP, we report preliminary studies of crystals of recombinant rabbit IRP1 bound to ferritin IRE. Diffraction data have been collected from several of the IRP1–IRE complex crystals and a complete native data set has been collected to 2.8 Å resolution.

2. Materials and methods

2.1. Protein expression and purification

Recombinant His-tagged IRP1$^{C437S/C503S}$ was engineered using an Altered Site mutagenesis kit (Promega Biotec; sequence **MGH-HHHHHADDDDDKDGVDKL**MSNPF . . . RKMAK, where the His-tag sequence is shown in bold). Mutations were confirmed by DNA sequencing. The protein was expressed in the protease-deficient *Saccharomyces cerevisiae* strain BJ5465 as described previously (Ke *et al.*, 1998). All purification procedures were performed at 277 K as follows. The yeast cell lysate was cleared by centrifugation at 20 000*g* for 60 min prior to being loaded onto a primed Ni-Chelating Sepharose Fast Flow (Amersham) column. IRP1 was eluted with 300 m*M* imidazole in 20 m*M* phosphate buffer, 500 m*M* NaCl pH 6.3, dialyzed against 5 m*M* NaCl in 20 m*M* Tris–HCl pH 8.5 and loaded onto a Bakerbond WP-Quat anion-exchange column (Mallinckrodt Baker Inc.). IRP1 was eluted with a linear 5–500 m*M* NaCl gradient in 20 m*M* Tris–HCl pH 8.5. Fractions containing IRP1 were pooled, dialyzed against 20 m*M* phosphate buffer pH 6.3 containing 5 m*M* NaCl and loaded onto a WP Carboxy-Sulfon cation-exchange column

(Mallinckrodt Baker Inc.). IRP1 was eluted with a linear 5–500 m*M* NaCl gradient in the same phosphate buffer. The purity and homogeneity of the sample was confirmed both by 7.5% SDS–PAGE (Laemmli, 1970) and Western blots (Towbin *et al.*, 1979; Burnette, 1981). The purified IRP1 was dialyzed against 20 m*M* Tris pH 7.4, 100 m*M* NaCl, 0.1 m*M* EDTA, 5 m*M* DTT, 10% glycerol and concentrated to 6 mg ml^{-1} using Vivaspin concentrators with 50 000 molecular-weight cutoff (Sartorius). The protein was stored in 0.5 ml aliquots at 193 K until further use.

2.2. IRE–IRP1 complex preparation

A 30-nucleotide ferritin IRE RNA oligomer (sequence GUUC-UUGCUUCAACAGUGUUUGAACGGAAC) was purchased from HHMI/Keck Biotech at Yale University and deprotected and desalted according to the manufacturer's guidelines. The purity was checked by PAGE on a 15% denaturing gel and detected by UV shadowing. All solutions for complex formation were prepared using RNase-free reagents and DEPC-treated water. IRP1$^{C437S/C503S}$ and IRE RNA were combined in equimolar ratios (3 μ*M* each) in 20 m*M* Tris pH 7.4, 50 m*M* NaCl and 0.1 m*M* EDTA and incubated on ice for 30 min. The IRP1–IRE complex was concentrated by ultrafiltration (Sartorius) and transferred to a low-salt buffer of 5 m*M* NaCl, 5 m*M* DTT, 0.1 m*M* EDTA and 20 m*M* Tris pH 7.4. The concentration of the IRP1–IRE complex was 16.5 mg ml^{-1}.

2.3. Crystallization

The complex samples were centrifuged at 20 000*g* for 30 min prior to crystallization attempts. Crystallization trials were carried out at 291 K using the hanging-drop vapor-diffusion method. Drops were prepared by combining the complex solution with precipitant in a 2:1 volume ratio and then equilibrating against 0.75 ml reservoir solutions. Crystal Screen I, Crystal Screen II and Natrix Screen (Hampton Research) were used for the initial screening conditions.

2.4. X-ray diffraction analysis

Crystals were harvested from the drops, soaked for 15–30 s in a cryoprotectant solution of 50 m*M* sodium acetate pH 5.06, 350 m*M* ammonium phosphate, 16.5% erythritol and 16.5% xylitol, mounted on nylon loops and flash-cooled by immersion in liquid N$_2$. X-ray diffraction data were collected at near liquid-N$_2$ temperature at the 22-ID beamline of the SER-CAT facility at the Advanced Photon Source, Argonne National Laboratory. Diffraction data were collected at a wavelength of 1.0722 Å using a MAR CCD detector. The data were indexed and scaled using both *HKL*2000/*SCALE-PACK* (Otwinowski & Minor, 1997) and *XGEN* (Howard, 1996).

3. Results and discussion

Initial attempts to crystallize IRP1 were performed with the wild-type apoprotein. This form of the protein failed to give crystals under any conditions tried. Analysis of the purified wild-type IRP1 revealed heterogeneity (multiple bands) on both SDS–PAGE and isoelectric focusing gels. A C437S single IRP1 mutant gave similar results. To overcome this problem, a C437S/C503S double mutant of IRP1 was generated. The IRP1$^{C437S/C503S}$ double mutant was expressed in a soluble form in *S. cerevisiae* and was purified to homogeneity in three steps. SDS–PAGE showed the purified protein to have a single band and a molecular weight of approximately 100 kDa (Fig. 1), which is in agreement with the predicted molecular weight of 100.8 kDa (98.5 kDa from IRP1 plus 2.3 kDa from the His tag). Purified
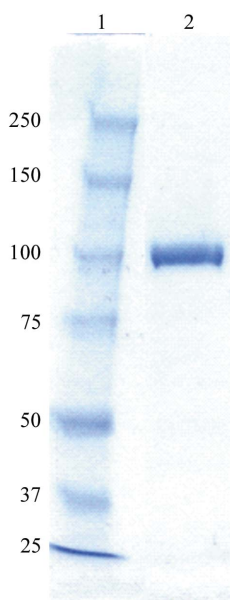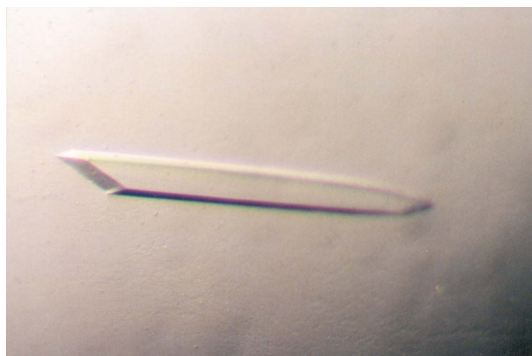

Figure 1
7.5% SDS–PAGE analysis of the C437S/C503S double mutant apo IRP1 after the final stage of purification. The apo IRP1 has been purified to homogeneity (lane 2). Molecular-weight markers are in lane 1 (numbers correspond to molecular weights in kDa).

Figure 2
Single crystal of the C437S/C503S double mutant IRP1 in complex with IRE. Crystals formed in one month by hanging-drop vapor diffusion, with drops containing 50 mM sodium acetate pH 5.06 and 220 mM ammonium dihydrogen phosphate equilibrated against 0.75 ml reservoirs of the same solution. The crystal dimensions were up to $40 \times 50 \times 300$ µm.

Table 1
Data-collection and processing statistics.

Values in parentheses correspond to the highest resolution shell (2.9–2.8 Å).

Space group	$P2_1$
Unit-cell parameters (Å, °)	$a = 109.6$, $b = 80.9$, $c = 142.9$, $\beta = 92.0$
Crystal-to-detector distance (mm)	200
Maximum resolution (Å)	2.8
Rotation for each exposure (°)	0.75
Time for each image (s)	6
Total rotation for data sets (°)	210
No. of measured reflections	188322
No. of unique reflections	57728
R_{merge}† (%)	11.2 (35.9)
Multiplicity	3.3 (3.4)
Completeness (%)	99.9 (97.9)
$I > 3\sigma(I)$ (%)	73.2 (52.8)
Average $I/\sigma(I)$	3.6 (1.7)

† $R_{merge} = \sum |I(h)_i - \langle I(h) \rangle| / \sum \langle I(h) \rangle$, where $I(h)_i$ is the observed intensity of the ith measurement of reflection h and $\langle I(h) \rangle$ is the mean intensity of reflection h calculated after merging and scaling.
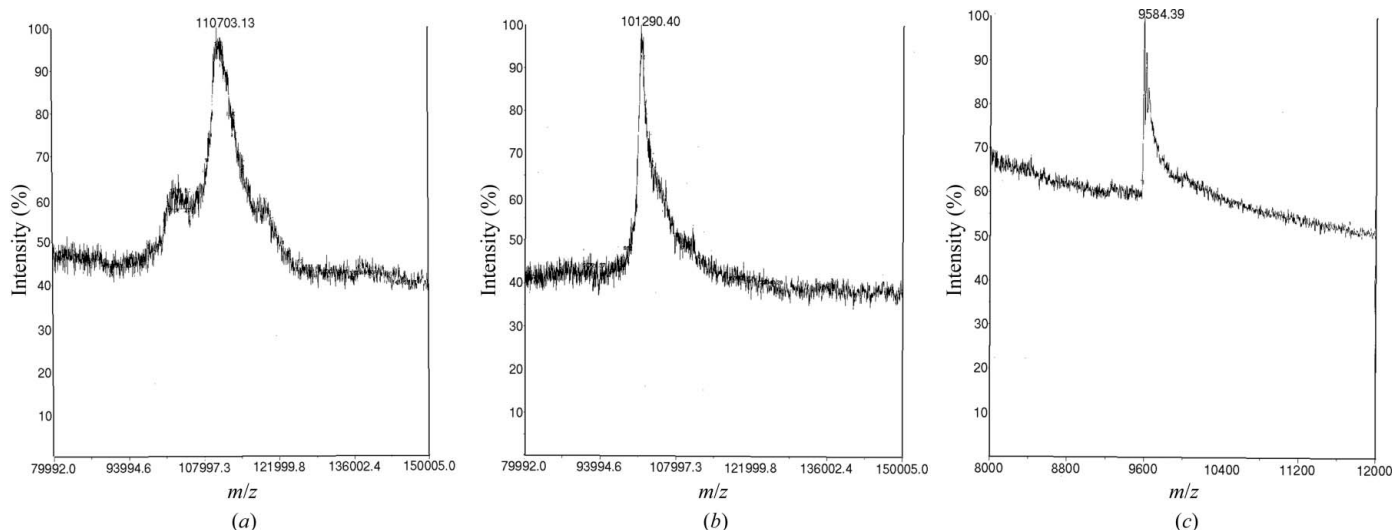
Figure 3
Mass-spectrometry results for contents of the crystals of the IRP1–IRE complex. (*a*) Freshly dissolved crystals, 110.70 kDa; theoretical MW of complex, 110.45 kDa. (*b*) Separated large component, 101.29 kDa; theoretical MW of IRP1, 100.83 kDa. (*c*) Separated small component, 9.584 kDa; theoretical MW of IRE, 9.623 kDa. The second peak in (*a*) corresponds to the mass of IRP1 alone, indicating partial separation during the mass-spectrometric experiment. Note that the His tag adds 2.32 kDa to the double mutant apo IRP1's MW of 98.51 kDa.

IRP1$^{C437S/C503S}$ retained IRE-binding activity (not shown), as expected from previous studies (Philpott *et al.*, 1994; Hirling *et al.*, 1994). Importantly, IRP1$^{C437S/C503S}$ did not show the heterogeneous behavior displayed by wild-type IRP1.

The sparse-matrix screening protocol (Jancarik & Kim, 1991) was used as a starting point in determining the optimal conditions for crystal growth at a constant temperature of 291 K. Apo-IRP1$^{C437S/C503S}$ alone produced twisted blade-like crystals that did not diffract. In contrast, the IRP1$^{C437S/C503S}$–IRE complex produced well formed needles in conditions of 0.4 M ammonium phosphate after two weeks. After further optimization, crystals suitable for X-ray diffraction were obtained in 50 mM sodium acetate pH 5.06 and 220 mM ammonium dihydrogen phosphate (Fig. 2). The dimensions of the single crystals were typically $20 \times 30 \times 300$ µm.

Mass spectrometry (DE-PRO-MALDI) was performed to address whether the crystals were of the IRP1–IRE complex. A single peak of 110.7 kDa was observed, which split into two peaks of 101.3 and 9.58 kDa upon conversion to 4% formic acid conditions (Fig. 3). The latter two species match the molecular weights of IRP1 and IRE, respectively. These results are strong evidence that these crystals are of the IRP1–IRE complex.

Various cryoprotectants were tried, including oils, PEG 400, glycerol, sucrose, erythritol and xylitol. The best results were obtained with soaking in a 1:1 mixture of erythritol and xylitol at 33% (16.5% each) for 15–30 s followed by flash-cooling by immersion in liquid N$_2$. Multiple data sets were collected. The crystals belong to the monoclinic space group $P2_1$, with unit-cell parameters $a = 109.6$, $b = 80.9$, $c = 142.9$ Å, $\beta = 92.0°$. Data-collection parameters and statistics are presented in Table 1.

The calculated packing parameter V_M (Matthews, 1968) for this crystalline form was 2.9 Å^3 Da^{-1}, corresponding to two complexes per asymmetric unit and a reasonable solvent content of 57% in the unit cell. Initial phase estimates were obtained by molecular replacement using domains of the c-aconitase structure (Dupuy *et al.*, 2006). Structure of the IRP1–IRE complex will give insights into the basis for the high specificity of the IRP1–IRE interaction and the mechanism of iron-modulated transformation of IRP1 between the c-aconitase and RNA-binding forms.

crystallization communications

References

Addess, K. J., Basilion, J. P., Klausner, R. D., Rouault, T. A. & Pardi, A. (1997). *J. Mol. Biol.* **274**, 72–83.

Brazzolotto, X., Timmins, P., Dupont, Y. & Moulis, J.-M. (2002). *J. Biol. Chem.* **277**, 11995–12000.

Burnette, W. N. (1981). *Anal. Biochem.* **112**, 195–203.

Dupuy, J., Volbeda, A., Carpentier, P., Darnault, C., Moulis, J. M. & Fontecilla-Camps, J. C. (2006). *Structure*, **14**, 129–139.

Eisenstein, R. S. (2000). *Annu. Rev. Nutr.* **20**, 627–662.

Gdaniec, Z., Sierzputowska-Gracz, H. & Theil, E. C. (1998). *Biochemistry*, **37**, 1505–1512.

Gunshin, H., Allerson, C. R., Polycarpou-Schwarz, M., Rofts, A., Rogers, J. T., Kishi, F., Hentze, M. W., Rouault, T. A., Andrews, N. C. & Hediger, M. A. (2001). *FEBS Lett.* **509**, 309–316.

Hirling, H., Henderson, B. R. & Kühn, L. C. (1994). *EMBO J.* **13**, 453–461.

Howard, A. J. (1996). In *Crystallographic Computing 7: Proceedings from the Macromolecular Crystallographic Computing School, 1996*, edited by P. E. Bourne & K. D. Watenpaugh. Oxford University Press.

Jancarik, J. & Kim, S.-H. (1991). *J. Appl. Cryst.* **24**, 409–411.

Ke, Y., Wu, J., Leibold, E. A., Walden, W. E. & Theil, E. C. (1998). *J. Biol. Chem.* **273**, 23637–23640.

Kennedy, M. C., Mende-Mueller, L., Blondin, G. A. & Beinert, H. (1992). *Proc. Natl Acad. Sci. USA*, **89**, 11730–11734.

Laemmli, U. K. (1970). *Nature (London)*, **227**, 680–685.

Matthews, B. W. (1968). *J. Mol. Biol.* **33**, 491–497.

Otwinowski, Z. & Minor, W. (1997). *Methods Enzymol.* **276**, 307–326.

Philpott, C. C., Klausner, R. D. & Rouault, T. A. (1994). *Proc. Natl Acad. Sci. USA*, **91**, 7321–7325.

Schalinske, K. L., Anderson, S. A., Tuazon, P. T., Chen, O. S., Kennedy, M. C. & Eisenstein, R. S. (1997). *Biochemistry*, **36**, 3950–3958.

Swenson, G. R. & Walden, W. E. (1994). *Nucleic Acids Res.* **22**, 2627–2633.

Theil, E. C. & Eisenstein, R. S. (2000). *J. Biol. Chem.* **275**, 40659–40662.

Towbin, H., Staehelin, T. & Gordon, J. (1979). *Proc. Natl Acad. Sci. USA*, **76**, 4350–4354.